INFLUENCE OF REINFORCED TRAILING EDGE ON FLAPPING WING AERODYNAMIC FORCE AND DEFORMATION

Yifan Wang[1], Bifeng Song[1,2], Yang Luo[1], Xinyu Lang[1], Wei Wang[1,2]

[1] School of Aeronautics, Northwestern Polytechnical University, Xi'an 710072, China
[2] National Key Laboratory of Aircraft Configuration Design, Xi' an 710072, China

Abstract

The deformation of the flapping wing is closely related to its lift and thrust. The influence of trailing edge stiffness of flapping wing on aerodynamic performance and deformation has not been deeply studied. In this paper, two different forms of flapping wings are studied experimentally. Wing deformation, including spanwise bend, spanwise twist, and trailing edge deflection deformation, was measured to compare the influence of reinforced wing on deformation. More thrust is generated by the wing with a reinforced trailing edge. The amplitude of the leading edge deflection of the strengthened wing is larger than that of the unreinforced wing. The average twist angle distribution is changed by the reinforced wing, and the average twist angle near the wing tip is smaller than that of the unreinforced wing. The change degree of the trailing edge deflection of the reinforced wing is faster.

Keywords: Flapping wings, Reinforced trailing edge, Aerodynamic force, Deformation

1. Introduction

Flying creatures in nature have excellent flying abilities. Inspired by bats, thin, pliable, and flexible membrane wings have attracted wide scientific interest.

Compared with rigid wings, flexible wings have unique characteristics. The comparison of deflection measurements by Rojratsirikul et al. [1] shows that the flexibility of membrane wings with low aspect ratio improves lift, while slightly reducing aerodynamic efficiency and reducing pitching moment at high angle of attack. These results suggest that membrane flexibility can reduce the effect of strong gusts by maintaining lift and reducing the effect of gusts on pitching torque. In their examination of flexible wings under steady state, A Song et al. [2] highlighted that although membrane wings exhibit limited aerodynamic efficiency in comparison to rigid flat plates at low to medium angles of attack, they possess the capability to delay stall and achieve a larger maximum lift coefficient. Y Lian et al. [3] and R E Gordnier et al. [4] have also reported that oscillations in flexible membranes result in a higher average lift. Pin Wu et al. [5] studied the wing rigidity by adding a skeleton to the wing with a half-span of 70mm and found that if the rigidity excessively inhibits the wing deformation during flapping, the propulsion efficiency of the wing will be reduced, that is, moderate deformation will bring better aerodynamic performance.

Different wing forms will bring different aerodynamic performance. P. Ifju et al. [6] studied a variety of wings with different stiffeners, trying to find better flight capability. R Albertani [7] compared the aerodynamic performance differences among rigid wing, chord-reinforced wing, and trailing-edge reinforced wing, and found that the trailing-edge reinforced wing has better lift performance.

During the flight of bats, their wings have complex deformation. In the research of S. Swartz [8], the deformation form of biofilm wing was studied by capturing the coordinates of the marking points stuck on bat wings. D. K. Riskin [9] used the same method to study the deformation angles of bat wings at different positions.

However, these studies have not studied the aerodynamic performance of different structural forms of bionic wings in an unsteady state and their deformation forms. In this paper, the differences in aerodynamic performance and deformation between the wing with reinforced trailing edge and the wing without reinforced trailing edge are studied through wind tunnel experiments.

2. Material and Method

2.1 Wing Configuration

The measured wing consists of carbon fiber stiffeners and a TPU membrane. The glue is reinforced with adhesive film and carbon fiber.

Two pairs of wings with different trailing edges are used in this experiment. The trailing edge of wing 1(W1) is not specially treated, and the film between the ribs of the two wings will be deformed. Wing 1 is shown in Figure 1 Wing (a). Figure 1 Wing (b) shows wing 2(W2), whose trailing edge is wrapped by carbon fiber stiffeners with a diameter of 0.6 mm. At the trailing edge of the wing, the deformation of the membrane is limited by stiffener. In addition, the stiffener increases the stiffness and weight of the trailing edge in the spanwise direction.

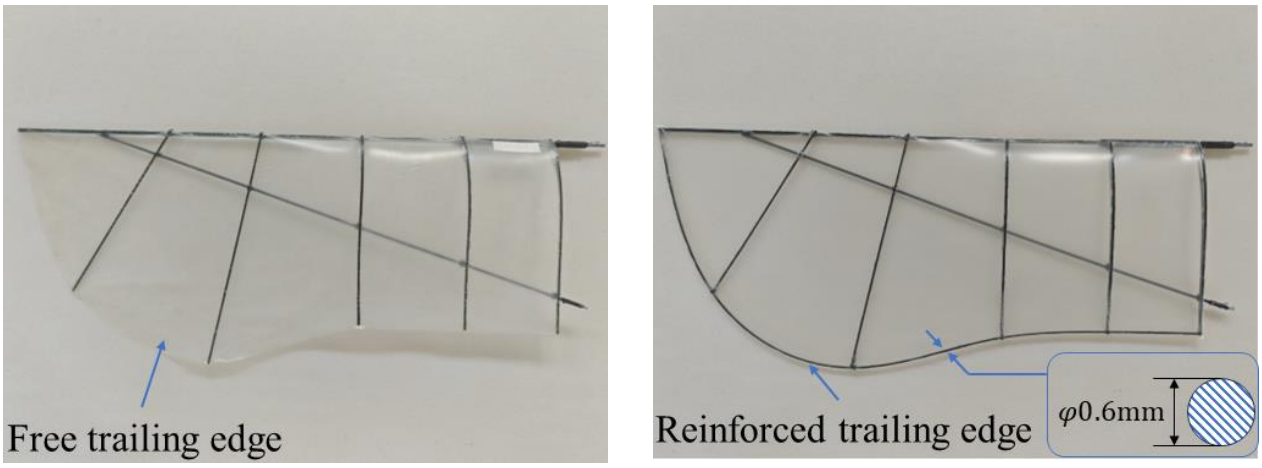

(a) (b)

Figure 1 Wing with different forms of trailing edge.

2.2 Experiment Setup

The experimental wind tunnel was carried out in an open low-speed straight-through wind tunnel of Northwestern Polytechnical University. The diameter of the test section is 1.6m, and the turbulence intensity of free flow is less than 0.5%. The average airflow deflection angle is less than 0.2, and the attack angle can be adjusted in the range of 10 ~ 20. The experimental device has a single-degree-of-freedom flapping wing mechanism. This mechanism is driven by a high-precision servo motor and can accurately perform flapping frequency within 30Hz with a flapping amplitude of 61 degrees. A six-component balance was used to measure lift and thrust. As a force measuring tool in this experiment, the mini40 balance has a resolution of 1/50N in the Z direction and 1/50N in the X direction.

The experimental device also includes a digital image correlation system, which consists of two high-speed cameras that can capture complete kinematics and structural deformation. Using the PHANTOM VEO-E-340L camera, the resolution is 1280×960 at the shooting speed of 500 frames. A 35mm fixed-focus lens was used for shooting.

Mark points of reflected light were attached to characteristic positions on the wing to track the three-dimensional coordinates of these positions. The location of marking points is indicated in 2.3. The markers were tracked manually in each frame using the DLTdv8, which is an open-source digitization tool developed by Hedrick[12].

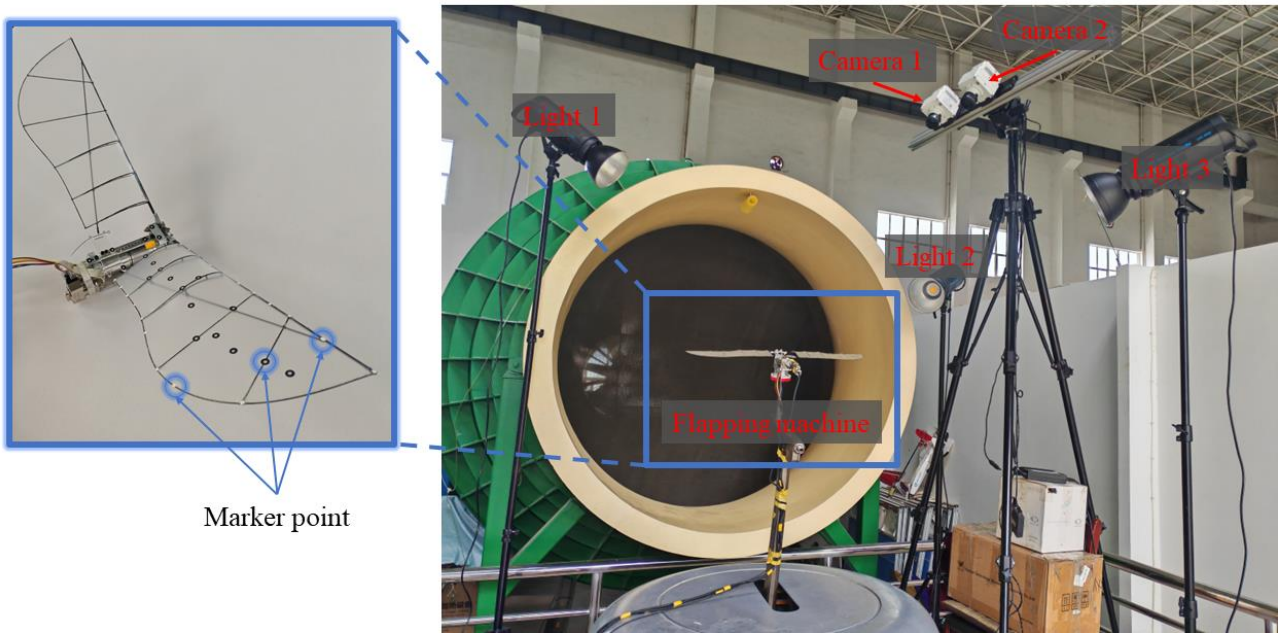

Figure 2 Experiment setup.

The experiment was carried out at 6m/s wind speed, the flapping frequency was 6Hz, and the angles of attack were 0° and 8°. The experimental Reynolds number is 40,000.

2.3 Deformation Definition

To evaluate the deformation difference between different wings, three expression methods of deformation characteristics are defined, as shown in Figure 2 Experiment setup.

Define an imaginary rigid plane, which is uniquely defined by two points at the wing root and the flapping origin. Deformation is defined as the relationship between a point on the actual airfoil and a rigid plane.

The vertical distance h between the point on the leading edge and the rigid plane is used to characterize the bending degree of the point. When the Z coordinate of the actual position is greater than the rigid plane, the bending is positive. On the contrary, bending is negative.

The twist angle θ is defined as the included angle between the chord and the flapping axis, that is, the X-axis. For the convenience of expression, the flapping axis* in the figure translates the flapping axis to the position of the measured section.

When the trailing edge is larger than the leading edge in the z-direction, the torsion angle is positive, and vice versa. The trailing edge warping deformation d is also defined as the distance of the trailing edge point from the rigid plane.

These deformations all reflect the deformation of the wing structure caused by aerodynamic load and inertia force. In this paper, the deformation at five given sections (0%R, 15%R, 34%R, 61%R, and 88%R), named C1, C2, C3, C4, and C5, was investigated.

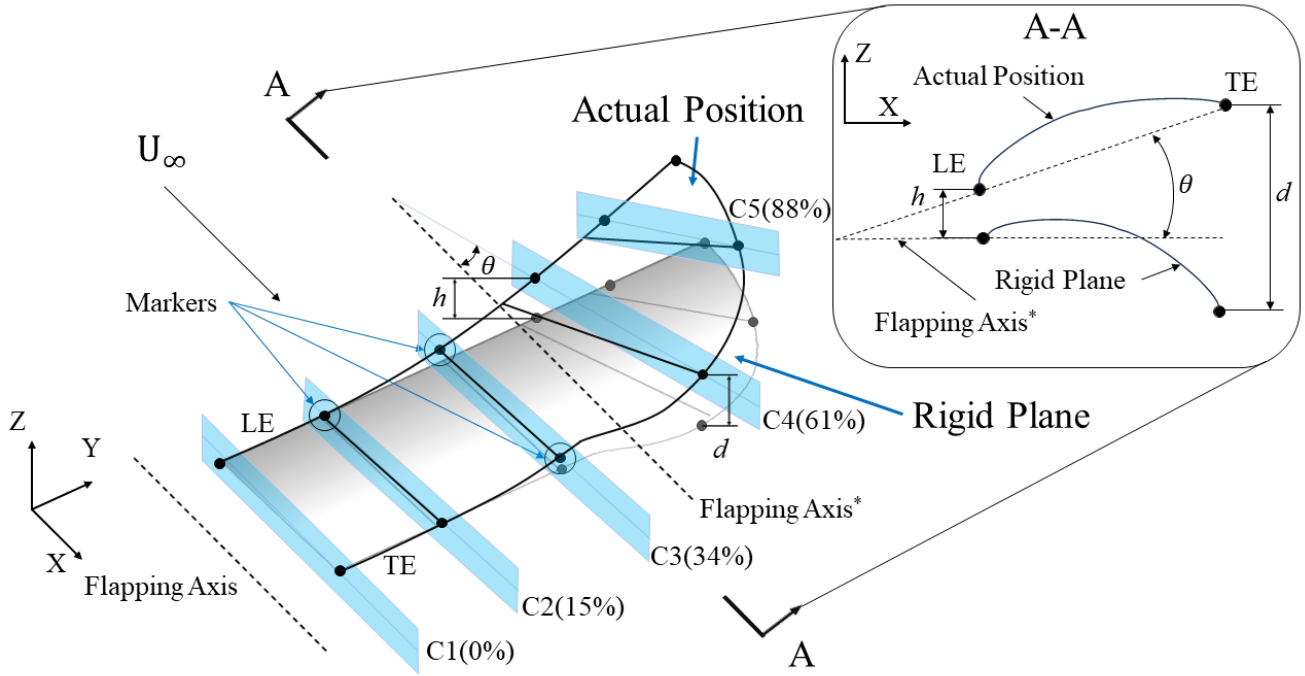

Figure 3 Deformation definition.

3. Aerodynamic Force

As shown in Figure 3, when the wing is horizontal, a coordinate system is established using the leading edge wing root position as the origin. The spanwise direction is denoted as the y-axis, the chord direction is denoted as the x-axis, and the vertical direction, that is, the direction perpendicular to the x-y plane, is the z-axis. The wing will swing around a rotating axis parallel to the x-axis, and the angle between the leading edge of the wing and the y-axis is defined as the flapping angle. The flapping angle of the wing is marked positive when it is moving in the positive direction of the z-axis, and negative when it is moving in the negative direction of the z-axis.

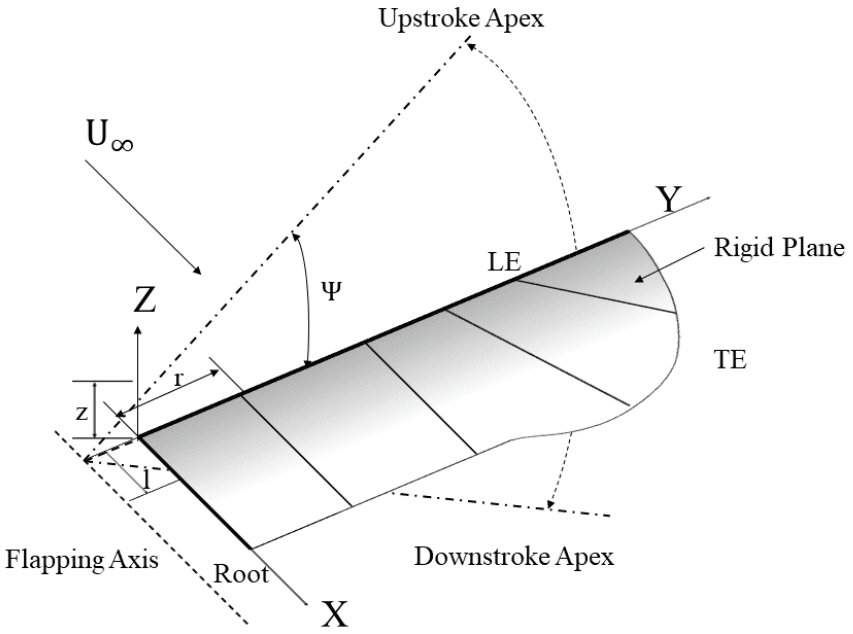

Figure 4 Flapping kinematics parameter definition.

According to this definition, the flapping angle was calculated by the flapping angle at practically every moment through the marked points on the leading edge. The transformation of the flapping angle over time in a period is shown in Figure 5. In the figure, time is normalized by cycles. The flapping angle changes almost a sine curve.

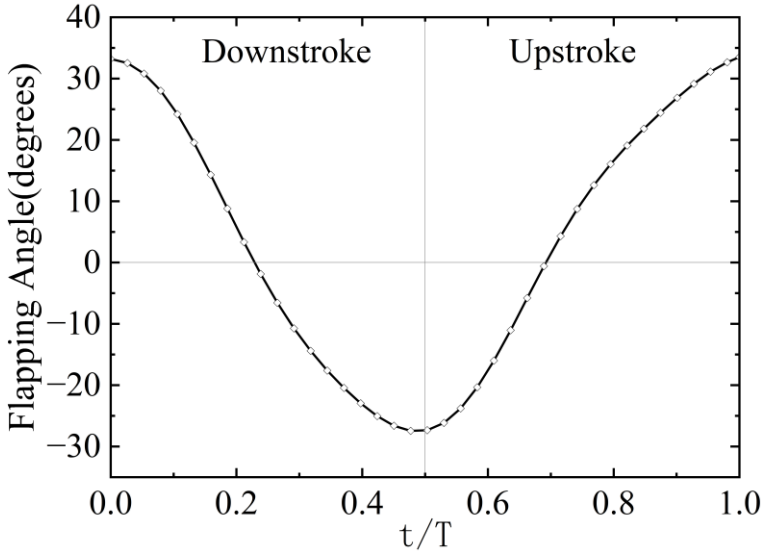

Figure 5 History of the flapping angle.

The instantaneous force is shown in Figure 5. The curve of a periodic force is intercepted. Figure 6 a) and Figure 6 b) represent the aerodynamic performance of W1 at 0° and 8°, respectively. Figure 6 c) and Figure 6 d) represent the aerodynamic performance of W2 at 0° and 8°.

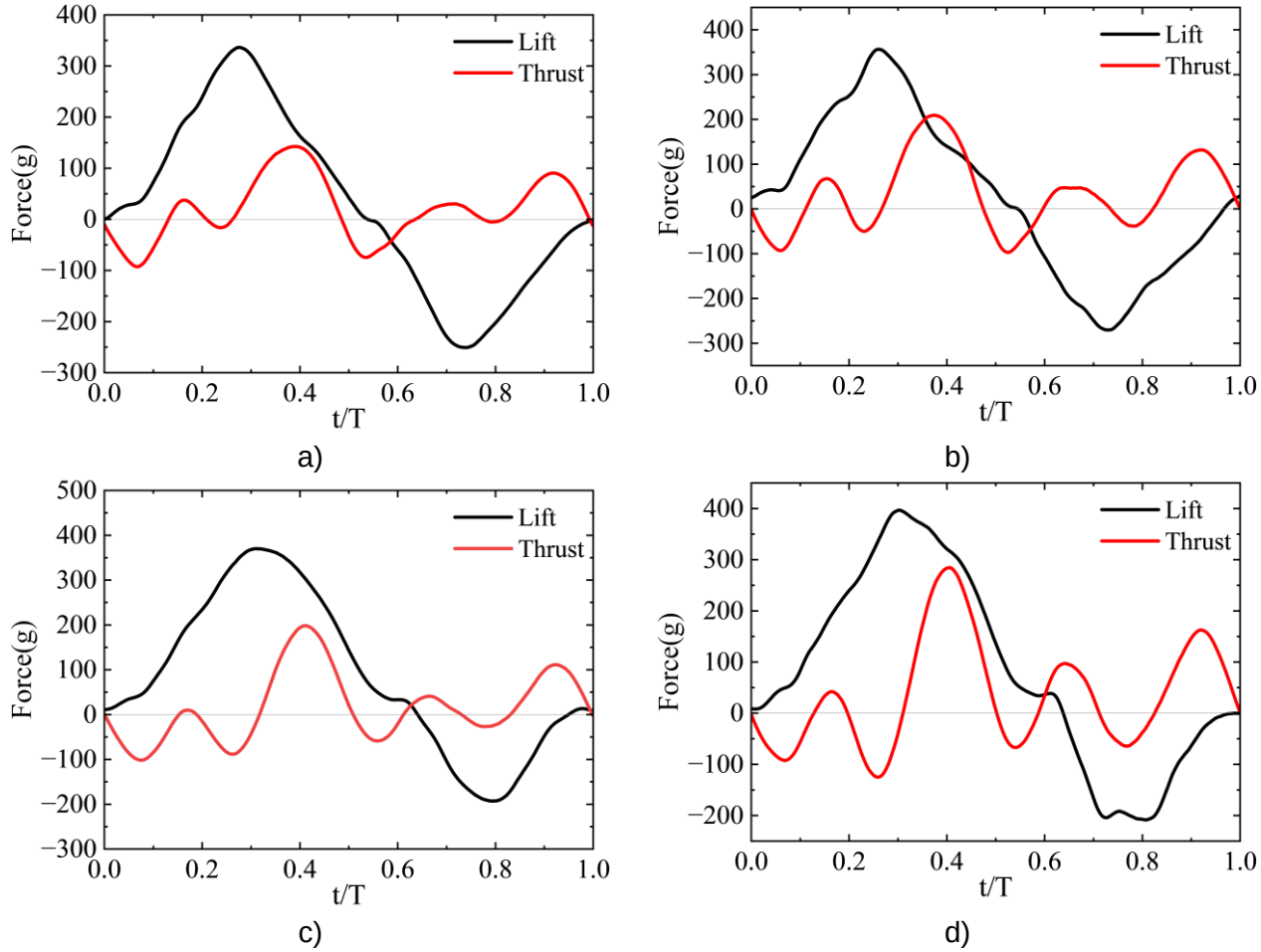

Figure 6 Instantaneous lift and thrust.

It can be seen that the lift curve has one crest and one trough, while the thrust curve has two peaks at half a cycle. The peak and trough values of W2 are greater than the force generated by W1 in the same state. Although the negative thrust generated by W2 is smaller than that of W1, the increase of positive thrust is higher at the same time, so W2 has better-thrust performance than W1.

The instantaneous lift and thrust in a period are averaged to obtain the average lift and thrust. The lift and thrust of each state are shown in Table 1. On the whole, the lift of the two wings increases with the increase of the angle of attack, and the thrust decreases with the increase of the angle of

attack. The lift performance of W1 is better than W2, but the thrust performance is worse than W2. At the angle of attack of 0, the lift ratio of W1 is increased by about 16% and the thrust is lost by 36%. At 8 angles of attack, the lift increased by 13% and the thrust decreased by 16%.

Table 1 Average lift and thrust

Force / AOA	W1		W2	
	Lift(g)	Thrust(g)	Lift(g)	Thrust(g)
0°	29.05	19.76	25.07	30.82
8°	84.64	15.07	74.88	27.79

4. Deformation

4.1 The Leading Edge Spanwise Bending Deformation

The degree of bending is constantly changing as the flapping progresses. Figure 7 shows the maximum, minimum, and average leading edge deflection. The circular point represents the leading edge deflection at the moment of maximum wing tip deformation in a flapping cycle, the diamond represents the value at the moment of minimum deformation, and the triangular point is the periodic average. These points are interpolated with cubic splines, and three flexural lines are obtained.

The shaded area is the area covered by the maximum and minimum values, that is, the area swept by the bend. Figure 7 a) and Figure 7 b) respectively show the leading edge bending deformation of W1 and W2 at the angle of attack of 0°. Figure 7 c) and Figure 7 d) respectively show the leading edge bending deformation of W1 and W2 at the angle of attack of 8°. When the angle of attack is 0°, all points on the maximum and minimum deflection curves of W1 are smaller than W2. At an 8° angle of attack, all points on the maximum and minimum deflection curves of W1 are greater than W2. At the same time, the minimum deflection amplitude of W1 at 0° angle of attack is greater than that of W2, while the minimum deflection amplitude at 8° angle of attack is smaller than that of W2.

The variation degree of each spanwise position of W2 in both states is greater than that of W1, that is, the difference between the maximum value and the minimum value of each position of W2 is greater than that of W1. The area swept by the deformation is shown in the figure as the area covered by the maximum deflection curve and the minimum deflection curve. W2 increases by 2.65% compared to W1 at 0° and by 17.51% at 8°. This indicates that the deformation of W2 is more severe at the leading edge.

In other words, the flapping amplitude of the wing increases due to elasticity during flapping, and eventually, the flapping amplitude of W2 is greater than that of W1. This greater amplitude may be due to increased trailing edge stiffness which increases the wing mass, making the W2 receive greater inertial forces.

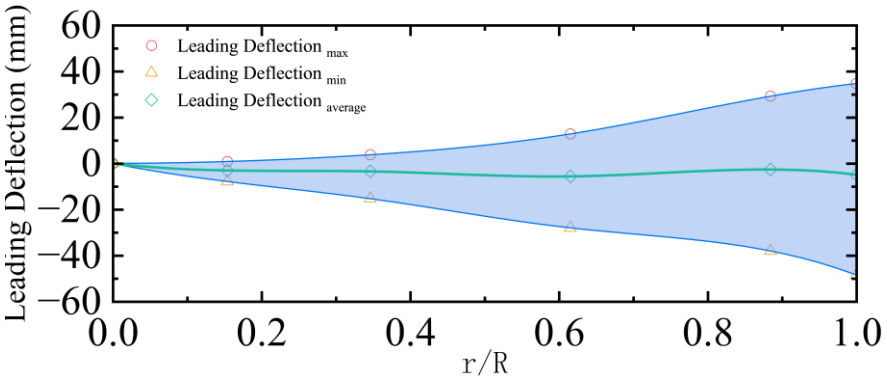

a)

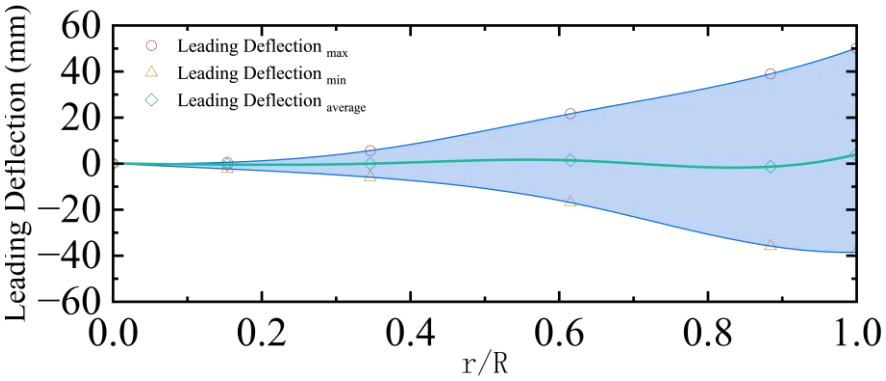

b)

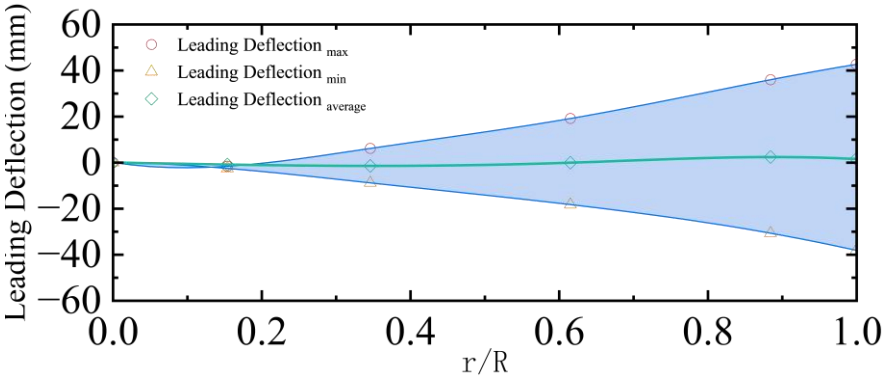

c)

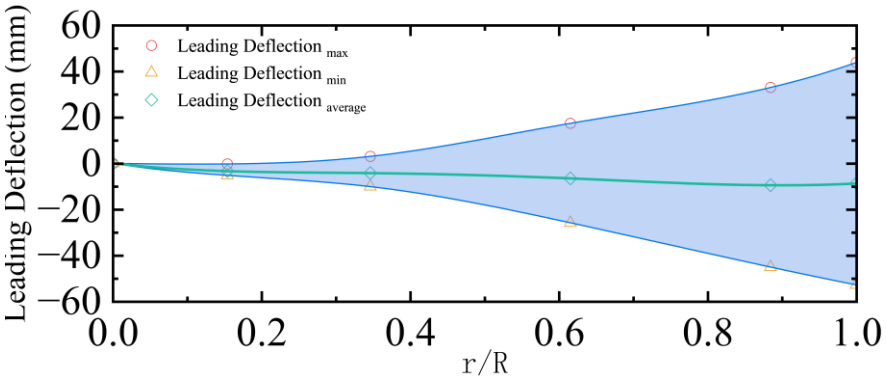

d)

Figure 7 The leading edge spanwise bending deformation.

4.2 Spanwise Twisting Deformation

Figure 8 shows the change of twist angle of each section with time in a cycle. Different cross sections are represented by solid lines and shapes of different colors. For comparison with the motion, the size of the flapping angle is shown by dotted lines. The dotted green line indicates the maximum point and the dotted red line indicates the minimum point.

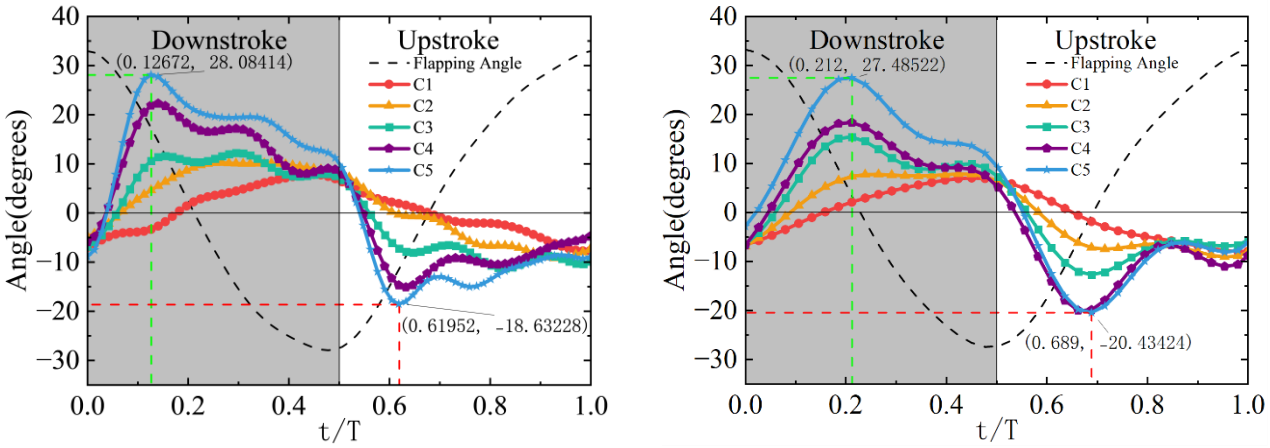

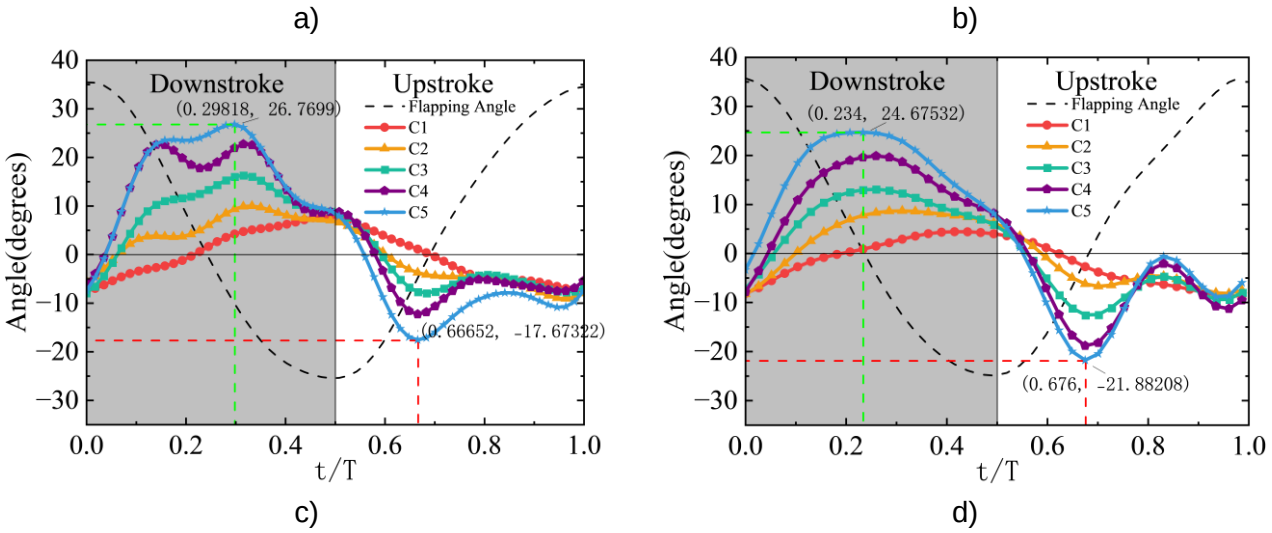

Figure 8 Twist angle of each section

At the end of the last cycle, that is, when the leading edge of the wing is at its highest point, the wing is about to swing down, and the twist angle of each section is in a negative state. During the downward flapping of the wing, the twist angle of each section begins to increase, and the increasing speed of the twist angle near the wing tip is greater. When the movement reaches about 0.03 cycles, the C5 and C4 sections first reach positive values, and then the twist angles of the C3 and C2 sections also reach positive values. However, C1 can reach a positive value later, because the deformation at the wing root is small and close to the active twist angle generated by the flapping mechanism. As the twist angle increases, the growth rate increases from the section at the wing root to the section at the wing tip. At about 0.13 cycles, the twist angles of C5, C4, and C3 sections reach their peak.

Because of the inertial force at play, the leading edge of the wing does not peak at the highest point of swinging since it continues to travel upward owing to inertia after it reaches its peak and begins to swing downward. The flapping angle's maximum lag is reached by the twist angle. At that point, the twist angle starts to drop, and it does so at a slower pace than it is growing. This is due to the aerodynamic stresses applied to the wings, which reduce the rate at which the twist angle changes.

Figure 8 a) and Figure 8 b) respectively show the changes in twist angles of each section of W1 and W2 when the angle of attack is 0°. From the figure, we can see that in the section near the wing tip, C5, C4, C3, and W1 reach the peak of positive twist angle before W2, and their difference is close to 0.1 flapping period. In peak size, W1 is slightly larger than W2. Next, during the reduction of the twist angle, the reduction process of W2 is smoother than that of W1, and a plateau appears at about 0.4 of the flapping period and then continues to decrease. The emergence of the platform may be due to the slowing down of the flapping mechanism. In contrast, W1 stagnated twice. This stagnation can be called a plateau.

The starting position of the uplap process and the initial position of the two pairs of wings are close to each other. The peak of W2 in the upstroke stage appears later than the initial position of the downstroke stage. At different times, the peak value of the twist angle of W2 is slightly larger than that of W1. In the following process, similar to the downstroke stage, the twist angle of W2 changes more smoothly, with one beat in the process of angle change, while W1 has multiple beats.

The leap in the up dive stage is a rebound as opposed to the stagnation of the down dive stage, and the twist angle reduces quickly after increasing. This is not the same as the downward dive procedure when the twist angle is continuously reduced. The twist angle stays reasonably constant because the flapping velocity is pretty steady and the aerodynamic load and inertial force balance out. The aerodynamic load is lowered, the flapping speed decreases, the equilibrium is upset, and the twist angle starts to drop even more as a result.

Figure 8 c) and Figure 8 d) respectively show the changes of twist angles of each section of W1 and W2 under the condition of Reynolds number at 110,000, flapping frequency at 6hz, and angle of attack at 8°. During the downstroke, the twist angle of both wings is different from that of 0 angles of attack. W1 showed two peaks with similar magnitudes. The first peak is close to the time when the peak below 0 angle of attack occurs. The second peak occurred close to 0.3 cycles, which coincided with the first stagnation phase at 0 angle of attack.

The peak of W2 appears later, and the change of twist angle near the peak is more moderate. As the flapping continued, W1 developed a stagnant area similar to the 0° angle of attack. W2 also had a slight tendency to stall, but this was quickly interrupted by the upsurge phase. In the upstroke stage, the change of W2 is the same as that at 0° angle of attack, but the change amplitude is a little larger. At the end of the jump stage, the twist angle of the section of the wing tip position is even close to 0°. The change of W1 is more moderate than the change of 0° angle of attack, and the twist angle appears a bounce.

We notice that the wings with different trailing edge stiffness have different characteristics in twist angle distribution. It can be seen from the change curve of the instantaneous twist angle that the twist angle of the two pairs of wings has different distribution characteristics. The twist angle of each section of W1 is close, while the difference between the C5 section and the C4 section of W2 is large. In addition, the peak of W1 is sharp, while W2 is relatively flat. Figure 9 shows the average of the twist angles of different orientation stations over a period, with the dashed line representing W1, the solid line representing W2, the red representing 0° and the black representing 8°.

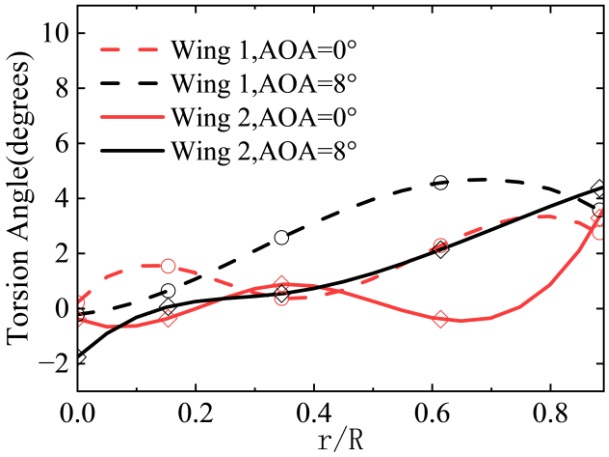

Figure 9 Mean twist angle

The two pairs of wings showed distinct trends. At different angles of attack, the peak of twist angle of W1 appears in the C4 section, that is, the maximum chord length section. Subsequently, the twist angle of the section begins to decrease. In contrast, the maximum twist angle of W2 appears at the wing tip and is a small value in the C4 section, which soon begins to increase.

Restricting the deformation at the place with a longer chord length is aided by increasing the stiffness of the trailing edge. Within the section twist angle of around 90% half span, the wings with greater trailing edge stiffness are all smaller than regular wings. And the hand wing is where this improvement is most noticeable. The idea states that the primary source of thrust creation is the hand wing portion. C4 and C5 sections of the experimental wing employed in this work can be regarded as hand wing pieces. These two sections' average twist angles demonstrate that greater thrust performance is correlated with smaller twist angles. This means that 0° is less than 8° and therefore W2 is smaller than W1.

This might be the cause of the increased thrust. In actuality, big effective angles of attack correlate with modest twist angles. The attack angle steadily reduces as the twist angle rises. Thus, a small mean twist angle causes that section's angle of attack to rise, which in turn causes thrust to increase. The force component in the thrust direction is increased by the wing tip's greater twist angle.

4.3 The Trailing Edge Deflection Deformation

Unlike the leading edge, the plane shape of the trailing edge is a curve. The deformation degree of the trailing edge is affected by the leading edge deformation, twist angle, and chord length of the section. Figure 9 shows the relationship of the trailing edge deformation of each section with time. Among them, Figure 9 a) and c) show the relationship between the trailing edge warping degree d of W1 at 0° and 8° angle of attack with flapping period, respectively. Figure 9 b) and d) show this feature of W2 at 0° and 8° angles of attack.

Similar to the change of twist angle, the deformation peak value lags behind the upper and lower limit positions. The difference is that the curvature of the posterior edge of the C4 and C5 sections is very close, but the distance from the other sections near the wing root is far. The main contributors to trailing edge warping deformation are C4 and C5 cross sections. In contrast, the C4 of W1 is

much closer to the C5 cross-section deformation, while W2 is relatively far away. This is because the strengthening of the trailing edge increases the stiffness of the trailing edge, so the deformation degree between the two sections is quite different.

Except for W1 at 8° angle of attack, the other states decline rapidly after the peak. Different from the obvious plateau when the twist angle changes, the trailing edge deformation has almost no plateau in the process of decline, only some weak trends. The reduction rate of W2 trailing edge deformation is faster than that of W1, which also makes W2 seem to have a more obvious plateau in the following process. But this stagnant trend was quickly replaced by a rapid decline in the upsurge phase.

When W1 is at an 8° angle of attack, the magnitude of deformation changes like the trend of twist angle change, there are two peaks of similar amplitude, and then it begins to decline. The decline was followed by a clear plateau that continued into the upsurge phase.

In the following upjump process, the peak value also lags behind a certain phase of the upjump process. The negative peak value of W2 is smaller than that of W1. Subsequently, the amount of deformation began to increase and a plateau appeared. The plateau of the W2 appears later, and the greater stiffness takes longer to balance the aerodynamic load.

Compared with the changing trend of twist angle, the change of trailing edge deformation looks smoother overall. There are fewer plateaus, and the process of change is smoother.

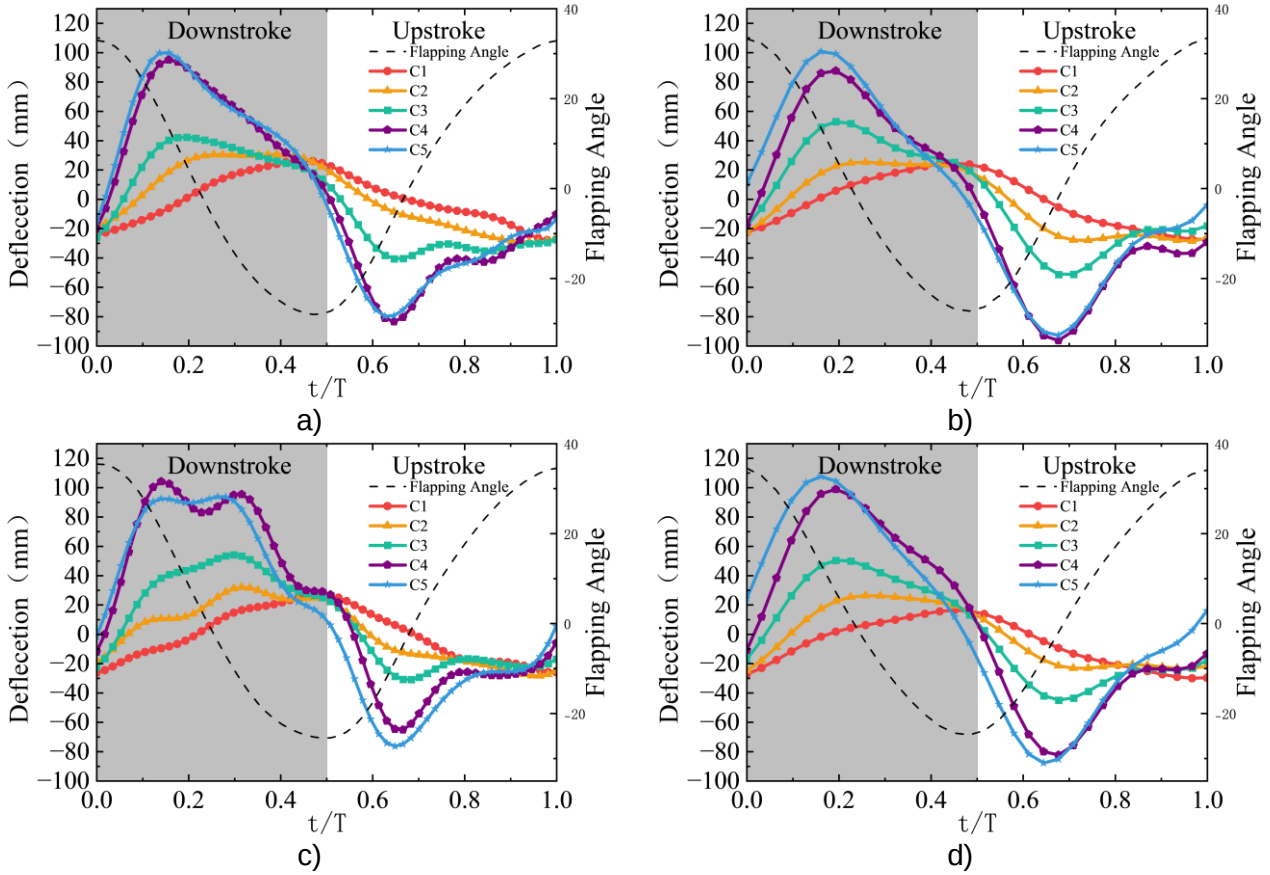

Figure 10 The trailing edge deflection deformation

5. Conclusion

In this paper, the deformation and aerodynamic performance of the flapping wings of imitation birds are evaluated based on the measured deformation in wind tunnel experiments. The effects of two pairs of different trailing edge stiffness on the deformation of the flapping wing at different angles of attack are studied. This study draws the following conclusions:

(1) Although the wing with higher trailing edge stiffness has a loss in lift performance, it has a significant advantage in thrust performance.

(2) The reinforced trailing edge has a certain influence on the amplitude of the leading edge deformation. A wing with higher trailing edge stiffness will produce a larger leading edge deformation amplitude.

(3) The twist angle of the wing presents two obvious peaks respectively in the upstroke and downstroke stages, and the two peaks of the twist angle of the wing with reinforced trailing edge are lower. In addition, wings with greater trailing edge stiffness have a smaller mean twist angle near the wing tip.

(4) The wing with high trailing edge stiffness rebounds faster after the trailing edge deformation reaches the extreme value, and the plateau stage appears later than the common wing in the upstroke process.

6. Contact Author Email Address

mailto: 1013425980@QQ.com

7. Copyright Statement

Acknowledgment

This paper is sponsored by the Innovation Foundation for Doctor Dissertation of Northwestern Polytechnical University (CX2024037)

References

[1] R. Bleischwitz, R. de Kat and B. Ganapathisubramani, "Aeromechanics of membrane and rigid wings in and out of ground-effect at moderate Reynolds numbers," *Journal of Fluids and Structures*, Vol. 62, pp. 318-331, 2016.

[2] A. Song, X. Tian, E. Israeli, R. Galvao, K. Bishop, S. Swartz, and K. Breuer, "Aeromechanics of Membrane Wings with Implications for Animal Flight," *AIAA Journal*, Vol. 46, pp. 2096-2106, 2008.

[3] Y. Lian, W. Shyy, D. Viieru, and B. Zhang, "Membrane wing aerodynamics for micro air vehicles," *Progress in Aerospace Sciences*, Vol. 39, pp. 425-465, 2003.

[4] R. E. Gordnier, "High fidelity computational simulation of a membrane wing airfoil," *Journal of Fluids and Structures*, Vol. 25, pp. 897-917, 2009.

[5] P. Wu, P. Ifju and B. Stanford, "Flapping Wing Structural Deformation and Thrust Correlation Study with Flexible Membrane Wings," *AIAA Journal*, Vol. 48, pp. 2111-2122, 2010.

[6] P. Ifju, D. Jenkins, S. Ettinger, Y. Lian, W. Shyy, and M. Waszak, "Flexible-wing-based micro air vehicles," *AIAA Aerospace Sciences Meeting & Exhibit*, 2002.

[7] R. ALBERTANI, B. STANFORD, J. P. HUBNER, and P. G. IFJU, "Aerodynamic coefficients and deformation measurements on flexible micro air vehicle wings," *Experimental Mechanics*, vol. 47, pp. 625-635, 2007.

[8] S. Swartz, J. Iriarte-Diaz, D. Riskin, X. Tian, A. Song, and K. Breuer, "Wing Structure and the Aerodynamic Basis of Flight in Bats," *AIAA Aerospace Sciences Meeting & Exhibit*, 2007.

[9] D. K. Riskin, D. J. Willis, J. Iriarte-Díaz, T. L. Hedrick, M. Kostandov, J. Chen, D. H. Laidlaw, K. S. Breuer, and S. M. Swartz, "Quantifying the complexity of bat wing kinematics," J*ournal of Theoretical Biology*, Vol. 254, pp. 604-615, 2008.

[10] T. L. Hedrick, "Software techniques for two- and three-dimensional kinematic measurements of biological and bio-mimetic systems," *Bioinspiration & biomimetics*, Vol. 3, p. 034001-034001, 2008.